JACS
JOURNAL OF THE AMERICAN CHEMICAL SOCIETY

ARTICLE

pubs.acs.org/JACS

Efficient Direct Electron Transfer with Enzyme on a Nanostructured Carbon Film Fabricated with a Maskless Top-Down UV/Ozone Process

Akio Ueda,[†,‡] Dai Kato,[†] Ryoji Kurita,[†] Tomoyuki Kamata,[§] Hiroaki Inokuchi,[∥] Shigeru Umemura,[§] Shigeru Hirono,[⊥] and Osamu Niwa*[,†,‡,∥]

[†]National Institute of Advanced Industrial Science and Technology, 1-1-1 Higashi, Tsukuba, Ibaraki 305-8566, Japan

[‡]Tokyo Institute of Technology, 4259 Nagatsuta-cho, Midori-ku, Yokohama 226-8503, Japan

[§]Chiba Institute of Technology, 2-17-1 Tsudanuma, Narashino, Chiba 275-0016, Japan

[∥]University of Tsukuba, 1-1-1 Tenno-dai, Tsukuba, Ibaraki 305-8571, Japan

[⊥]MES-Afty Corporation, 2-35-2 Hyoe, Hachioji, Tokyo 192-0918, Japan

Supporting Information

ABSTRACT: We have developed a new carbon film electrode material with thornlike surface nanostructures to realize efficient direct electron transfer (DET) with enzymes, which is very important for various enzyme biosensors and for anodes or cathodes used in biofuel cells. The nanostructures were fabricated using UV/ozone treatment without a mask, and the obtained nanostructures were typically 2−3.5 nm high as confirmed by atomic force microscopy measurements. X-ray photoelectron spectroscopy and transmission electron microscopy revealed that these nanostructures could be formed by employing significantly different etching rates depending on nanometer-order differences in the local sp^3 content of the nanocarbon film, which we fabricated with the electron cyclotron resonance sputtering method. These structures could not be realized using other carbon films such as boron-doped diamond, glassy carbon, pyrolyzed polymers based on spin-coated polyimide or vacuum-deposited phthalocyanine films, or diamond-like carbon films because those carbon films have relatively homogeneous structures or micrometer-order crystalline structures. With physically adsorbed bilirubin oxidase on the nanostructured carbon surface, the DET catalytic current amplification was 30 times greater than that obtained with the original carbon film with a flat surface. This efficient DET of an enzyme could not be achieved by changing the hydrophilicity of the flat carbon surface, suggesting that DET was accelerated by the formation of nanostructures with a hydrophilic surface. Efficient DET was also observed using cytochrome *c*.

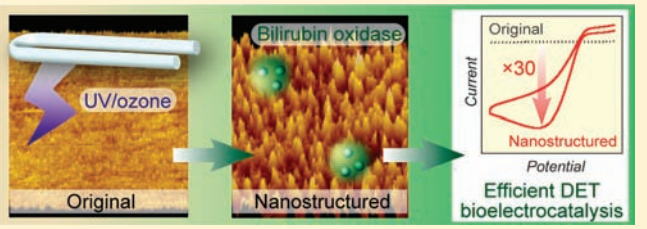

INTRODUCTION

Nanocarbon electrodes such as carbon nanotubes (CNTs) and mesoporous carbon (MC) have been studied with a view to greatly increasing their surface areas and thus their capacitance or increasing the amount of immobilized catalyst (e.g., metal nanoparticles or enzymes) on the electrodes. Immobilized enzymes on nanocarbon electrodes are expected to facilitate the direct access of electrons to/from enzyme redox centers,[1−5] which is very important for realizing biofuel cells and highly sensitive biosensors with a much simpler system (or structure). Willner's group has reported the use of nano-order materials, such as metal nanoparticles and carbon nanotubes, to achieve electrical contact with enzyme electrodes.[2,6] These types of modified electrodes have been studied for application in various enzyme biosensors.[7,8]

These metal nanoparticle and nanocarbon materials have mainly been prepared using a bottom-up process and therefore must be immobilized on solid substrates such as glassy carbon (GC) or metal substrates for use as sensor electrode platforms because they are typically powder or fiber-like structures.

In contrast, nanosized structures[9−11] could be fabricated with a top-down process using carbon films such as boron-doped diamond (BDD) films, which have been studied because of their excellent electrochemical characteristics. These characteristics include a low background current, a wide potential window, and good mechanical strength and chemical stability in comparison with CNT or MC materials.[12,13] Yang et al.[10,11] reported a vertically aligned nanowire formed from a BDD electrode that they realized by using reactive ion etching (RIE) with O_2 plasma after masking the surface with randomly cast diamond nanoparticles. They then applied the electrode to electrochemical DNA sensors with a detection limit in the picomolar range.[11] However, a harsh plasma process and a nanometer-sized mask are essential for etching of a robust sp^3 crystal region to form nanostructures on BDD films.

In contrast, the edge plane of sp^2 carbon has a high electrochemical activity for biomolecules. A nanosized structure on an

Received: September 24, 2010
Published: March 08, 2011

dx.doi.org/10.1021/ja108614d | J. Am. Chem. Soc. 2011, 133, 4840–4846

sp^2-rich carbon material could provide better electrochemical performance than sp^3 carbon. Recently, we reported an electron cyclotron resonance (ECR)-sputtered nanocarbon film consisting of an sp^2/sp^3 hybrid structure that exhibits excellent electrochemical performance for various biomolecules.[14−16] A nanosized surface structure could be more easily fabricated from our nanocarbon film than from a BDD film by using a top-down process because the sp^2/sp^3 ratio of our carbon film differs in nanoscale-level local areas.[14] This nanolevel inhomogeneous structure could allow us to form three-dimensional nanosized structures by utilizing a different etching rate in each nano-order region without the need for any mask materials. Moreover, the size of the nanosized surface structure could be controlled because the $sp^2/(sp^2 + sp^3)$ ratio of nanocarbon can be tuned by controlling the bias energy during film deposition. No fabrication concept based on a structure-dependent difference in the etching rate has been reported to date.

Here we demonstrate the maskless fabrication of nanosized structures on the surface of our nanocarbon film with a mild etching process by employing the etching rate difference induced by nanometer-order differences in the local sp^3 content. Instead of a plasma technique, we employed a UV/ozone process with a low-pressure Hg lamp for mild etching in ambient air to form nanosized structures on a carbon surface. To clarify the mechanism of etching of carbon materials with the UV/ozone technique, we used atomic force microscopy (AFM) and X-ray photoelectron spectroscopy (XPS) to evaluate the surface structure and $sp^2/(sp^2 + sp^3)$ ratio, respectively, for both our nanocarbon film and other carbon materials with different $sp^2/(sp^2 + sp^3)$ ratios or micro- or nanometer-level structures. These materials included GC, pyrolyzed polymers (PP) based on spin-coated polyimide or vacuum-deposited phthalocyanine films, diamond-like carbon (DLC), and BDD before and after UV/ozone treatment. We then used this carbon film to realize efficient direct electron transfer (DET) between an enzyme and a nanostructured electrode, which is a very important function for various enzyme biosensors and enzyme electrode-based biofuel cells.[2,6,17−21] We observed the DET efficiencies of bilirubin oxidase (BOD) and cytochrome *c* (cyt *c*) for a nanostructured carbon film fabricated with the UV/ozone process. In addition, we also compared the DET efficiencies of BOD and cyt *c* for the original flat films and nanostructured carbon films with various wettabilities.

EXPERIMENTAL SECTION

Chemicals. All of the chemicals were analytical-grade and used as received. Hexaammineruthenium(III) chloride, ammonium iron(II) sulfate hexahydrate, and dopamine hydrochloride were purchased from Sigma-Aldrich. Potassium ferricyanide was obtained from Wako Pure Chemical Industries, Ltd. (Japan). Potassium chloride was purchased from Kanto Chemical Co., Inc. (Japan). Perchloric acid and sulfuric acid were obtained from Nacalai Tesque, Inc. (Japan). Ultrapure water (Milli-Q) was used in all of the experiments. BOD (EC 1.3.3.5) and cyt *c* (from horse heart) were obtained from Sigma-Aldrich.

UV Treatment for Carbon Materials. Nanocarbon films were deposited onto silicon substrates by ECR sputtering.[14] The advantage of this method is highly controllable ion irradiation of the growing surface during deposition. For the sputtering, the argon pressure was 5.0×10^{-2} Pa and the substrate temperature was room temperature. The irradiation ion current density was 5.8 mA cm^{-2}, and the ion acceleration voltage ranged from 20 to 75 V. The film thickness was ~40 nm. A low-pressure Hg lamp (EUV110GS-36 L) for the UV/ozone treatment was purchased from SEN Lights Corp. (Japan). Various carbon materials, including nanocarbon, GC (P-1 GC Plate, BAS Co., Ltd., Japan), PP films prepared from polyimide or phthalocyanine films (NTT Advanced Technology, Japan), DLC (Nanotech Co., Japan), and BDD (SHMF-12730, Sumitomo Electric Industries, Ltd.), were placed under a low-pressure Hg lamp that provided 185 and 254 nm UV illumination (40 mW/cm^2 at 254 nm measured at the sample surface).

Carbon Film Characterization. C 1s and O 1s XPS spectra were recorded using a Shimazu/Kratos model AXIS Ultra spectrometer (Al Kα, 1486.6 eV) to determine the elemental composition and the number of chemical bonds in the carbon electrode surfaces. AFM measurements were performed with an SPI4000 atomic force microscope (SII NanoTechnology, Inc.) using a silicon cantilever in air at room temperature. The images were recorded in the dynamic force AFM mode at a scan rate of 0.3 Hz and a resolution of 256 × 256 pixels.

Electrochemical Measurements. All of the electrochemical experiments were performed using an ALS/CHI 730C electrochemical analyzer (CH Instruments, Inc.). A platinum wire and a Ag/AgCl (3 M NaCl) electrode (BAS) were used as auxiliary and reference electrodes, respectively.

DET Measurements for BOD and Cyt *c*. BOD was dissolved in a pH 7.0 phosphate buffer (PB). To achieve the physical adsorption of BOD on the nanocarbon surface, the carbon substrate was immersed in 1 mg/mL BOD for 1 h and then rinsed with PB solution. The electrode was then transferred to a PB solution for CV measurements. In the cyt *c* measurements, the CV was obtained using 100 μM cyt *c* dissolved in PB (pH 7.0).

RESULTS AND DISCUSSION

Fabrication and Characterization of the Nanostructured Carbon Film Obtained Using the UV/Ozone Process. We obtained AFM images of the topographical changes on the nanocarbon film before and after UV/ozone treatment, as shown in Figure 1A−C. The surface of the 40 nm thick as-deposited carbon film with an average roughness (Ra) of 0.6 Å changed to a rougher and homogeneously distributed thornlike nanostructure. The nanostructure density on the carbon film was ~350 μm^{-2} after a 3 h treatment (Figure 1D). Further treatment exposed the Si substrate. The etching rate was ~7 nm h^{-1} when the low-pressure Hg lamp intensity at 254 nm was 40 mW cm^{-2} at the surface. During Hg lamp irradiation in air, O_2 absorbs the 185 nm UV light and forms ozone. The ozone then absorbs the 254 nm UV light and decomposes into singlet oxygen molecules.[22] Typically, both of these oxidants and the UV energy affect the sample surface. To clarify the nanocarbon etching mechanism with the UV/ozone technique, we treated the nanocarbon with UV irradiation under the following conditions:

1. UV treatment at 185 and 254 nm in a N_2 flow to supply the nanocarbon surface with UV energy under non-ozone conditions.
2. UV treatment at 185 and 254 nm while increasing the distance between the Hg lamp and the nanocarbon film surface from 500 to 1000 μm to reduce the UV intensity at the nanocarbon surface.

Under conditions 1, no topographical change was observed with the AFM measurement, and the nanocarbon film thickness remained unchanged, indicating that the use of UV energy without ozone has little effect on the nanocarbon film structure. However, the $sp^2/(sp^2 + sp^3)$ ratio changed from 0.6 to 0.53 after UV/ozone treatment. By comparison with the $sp^2/(sp^2 + sp^3)$ ratio of 0.4 shown in Figure 2 when the nanocarbon was

dx.doi.org/10.1021/ja108614d | J. Am. Chem. Soc. 2011, 133, 4840–4846

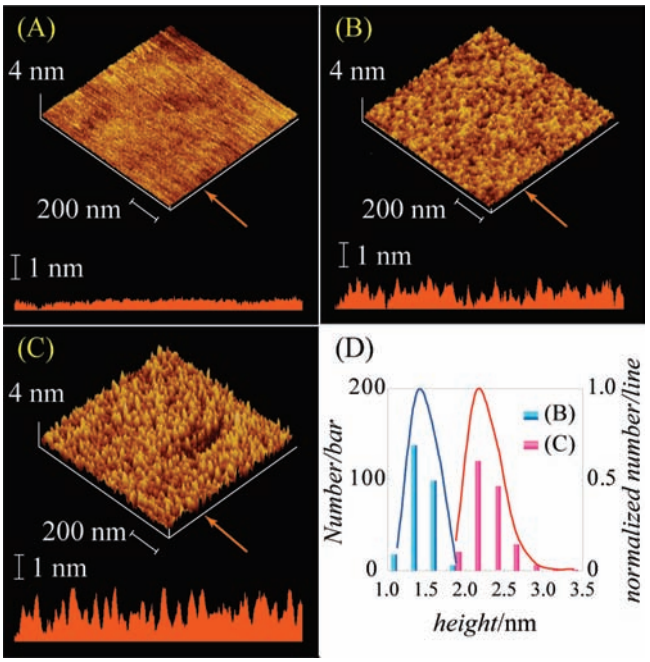

Figure 1. (A−C) AFM topographical images and height line profiles at points indicated by the arrows: (A) before UV/ozone irradiation; (B) after irradiation for 1.5 h; (C) after irradiation for 3 h. (D) Relationship between thorn height and number in (B) and (C).

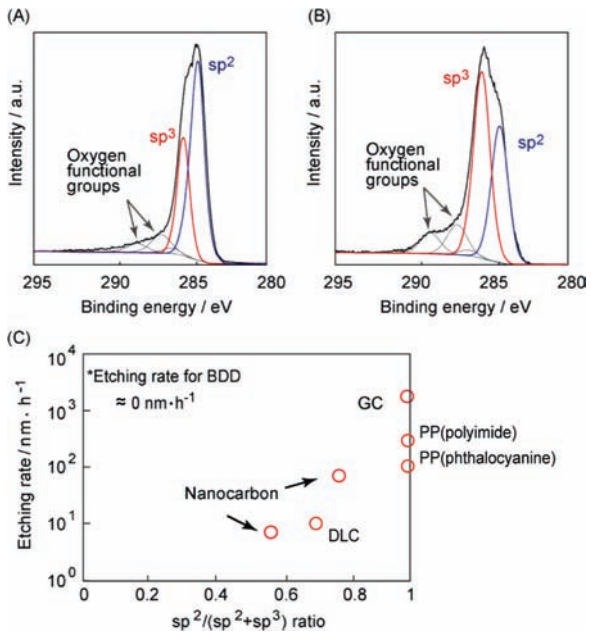

Figure 2. C 1s spectra of nanocarbon film (A) before and (B) after UV/ozone irradiation for 3 h. (C) Relationship between the $sp^2/(sp^2 + sp^3)$ ratio and the etching rate.

treated with UV in air, this change was much smaller and thus could have been caused by a small quantity of oxygen and/or water molecules in the N_2 flow that was converted to ozone. This is because it was very difficult to completely remove adsorbed oxygen and water from the nanocarbon and the inside of the chamber simply with a N_2 flow at ambient pressure. Under conditions 2, the topography was slightly rougher than that of the

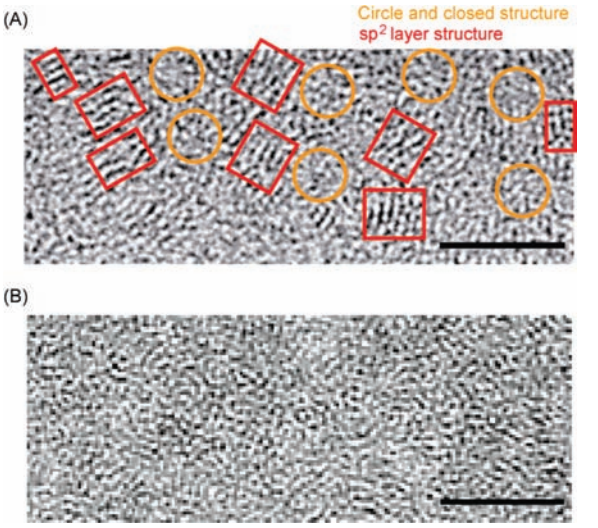

Figure 3. TEM images of (A) nanocarbon with an $sp^2/(sp^2 + sp^3)$ ratio of 0.6 and (B) a commercially available DLC film. Scale bar = 5 nm.

original nanocarbon surface, as shown in Figure S1 in the Supporting Information. The Ra increased from 0.6 to 3.5 and 2.2 Å for distances of 500 and 1000 μm, respectively, between the Hg lamp and the sample. Since the intensity of the 185 nm light that was absorbed by O_2 decreased progressively with increasing distance, this lower Ra value is due to the lower ozone concentration at the sample. Therefore, in our case, this relatively high power was important in regard to etching the nanocarbon, since we could not observe such topographical changes at 10 mW cm^{-2}, which is a typical intensity for UV/ozone treatment.[23] The XPS spectrum indicated that the surface O/C ratio increased from 0.05 to 0.14 after the UV/ozone treatment (Figure S2). This was because the ozone or singlet oxygen molecules etched the carbon surface and finally formed oxygen-containing groups on the carbon surface.

C 1s spectra, which include surface sp^2 and sp^3 bond components,[24,25] revealed that the $sp^2/(sp^2 + sp^3)$ ratio fell from 0.6 to 0.4 (Figure 2). To clarify the effect of the UV/ozone process on the sp^2 and sp^3 bonds in carbon materials, we also treated other carbon materials with various $sp^2/(sp^2 + sp^3)$ ratios, including GC, PP, DLC, and polycrystalline BDD, with the same UV/ozone process (AFM images are shown in Figure S3). The thornlike structure observed for our UV/ozone-treated nanocarbon could not be confirmed in these carbon materials. Moreover, we also used ECR sputtering to prepare a nanocarbon film with a lower sp^3 content [$sp^2/(sp^2 + sp^3)$ ratio = 0.8] and obtained an etching rate of 70 nm h^{-1}. We observed a similar nanostructure for this film, as shown in Figure S3F.

The relationship between the etching rate and the $sp^2/(sp^2 + sp^3)$ ratio is shown in Figure 2C, which indicates that an increase in the sp^3 component exponentially reduces the etching rate. However, the thornlike structures were observed only for nanocarbon films with $sp^2/(sp^2 + sp^3)$ ratios of 0.6 and 0.8. (Figure 1 and Figure S3). Figure 3A shows a transmission electron microscopy (TEM) image of our nanocarbon film with an $sp^2/(sp^2 + sp^3)$ ratio of 0.6. One of the authors has reported that the number of circular and closed structures with sizes of ~5 nm seen in the TEM image increases when the $sp^2/(sp^2 + sp^3)$ ratio decreases from 0.8 to 0.6.[14] Such a structure could contain more sp^3 bonds and corresponds to the thorn width

dx.doi.org/10.1021/ja108614d |J. Am. Chem. Soc. 2011, 133, 4840–4846

observed with AFM. In contrast, no such nano-order structure could be observed in the TEM image of commercially available DLC or previously reported DLC[26,27] (Figure 3B). In fact, a thornlike nanostructure did not form on the commercially available DLC film after UV/ozone treatment, as shown in Figure S3E. These results indicate that the nanostructure after UV treatment depends on not only the internal carbon sp^2/sp^3 ratio but also specific nano-order structures as seen in TEM images. Ferrari and Robertson[28] have reported a ternary phase diagram including sp^2, sp^3, and hydrogen of amorphous carbons. This diagram is useful for conventional DLC with an amorphous structure. However, they mentioned that the degree of clustering of the sp^2 phase should be added as a fourth dimension. Such clusters, especially sp^3-rich clusters dispersed in sp^2-rich clusters, may be necessary for fabrication of the nanostructure using the UV/ozone technique. This is because sp^3-rich clusters have a lower etching rate than sp^2-rich clusters, and the thornlike nanostructure could result from a nanometer-order difference in the etching rates for the two different domains. Since the average etching rate of the carbon film was 7 nm h^{-1} and the maximum height difference was 2−3.5 nm after a 3 h treatment, the difference in the local etching rate of the carbon film was only 9.5−16.7%, which corresponds to a difference of only 1−2% in the local sp^3 content as calculated using the results in Figure 3A. We also employed other etching techniques such as oxygen plasma and electrochemical oxidation on the nanocarbon in an attempt to fabricate thornlike nanostructures. However, we could not fabricate such nanostructures with those techniques (Figure S4). This indicates that the etching rate difference does not depend on the sp^2 and sp^3 bond content when those techniques are used because their high oxidation energy eliminates the selective etching properties.

Electrochemical Properties of the Thornlike Nanocarbon Film. We measured the basic electrochemical properties of the thornlike nanostructured carbon film to evaluate the efficiency of the nanostructure. The capacitance value (C^0) and electrochemical activity of redox species on the thornlike nanostructured carbon film were studied by cyclic voltammetry (CV). The C^0 values of the original and nanostructured carbon, measured by CV at 0.25 V vs Ag|AgCl in 1 M KCl,[29] were 12.3 and 34.1 μF cm^{-2}, respectively. This was due to the increase in both the electrode area and the number of surface oxygen functional groups.[1]

Voltammograms that we obtained for the redox species $Ru(NH_3)_6^{2+/3+}$, $Fe(CN)_6^{3-/4-}$, $Fe^{2+/3+}$, and dopamine (DA) on the original and nanostructured carbon films are shown in Figure 4. Voltammograms for $Ru(NH_3)_6^{2+/3+}$, which is an outer-sphere-type redox species, exhibited an almost reversible electrochemical response on both carbon films, as shown in Figure 4A. Although the UV/ozone treatment partly reduced the sp^2 content of the carbon material, the nanostructured carbon film had a sufficient number of sp^2 bonds exhibiting high electrochemical activity in this current range and sufficient conductivity without interference from the current−resistance (IR) drop.

In fact, the electron transfer rate of $Fe(CN)_6^{3-/4-}$ (which is sensitive to the surface state, especially the sp^2 edge plane site[30,31]) increased and the value of ΔE_p decreased from 160 to 68 mV after the UV/ozone treatment of the nanocarbon film, as shown in Figure 4B. The UV/ozone treatment increased the number of surface sp^2 edge sites despite the decrease in sp^2/sp^3 ratio because of the increase in surface area of the nanostructure.

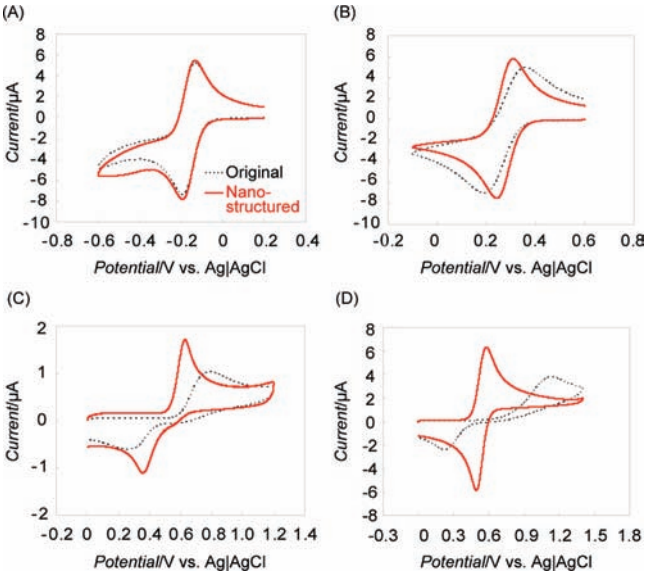

Figure 4. Voltammograms of redox systems on the original and thornlike carbon electrodes: (A) 1 mM $Ru(NH_3)_6^{3+/2+}$ in 1.0 M KCl; (B) 1.0 mM $Fe(CN)_6^{3-/4-}$ in 1.0 M KCl; (C) $Fe^{2+/3+}$ in 0.1 M $HClO_4$; (D) 0.1 mM DA in 0.1 M $HClO_4$. Scan rate = 100 mV s^{-1}.

This high electron transfer rate for $Fe(CN)_6^{3-/4-}$ on the nanostructured carbon film is totally different from the relatively low electron transfer rate for a BDD-based nanowire,[11] since the electrochemical activity of BDD is attributed to boron doping sites and a small sp^2 boundary region, which is typically 0.05% of the microcrystalline BDD surface.[32,33] The value of ΔE_p decreased from 910 to 85 mV after UV/ozone treatment for $Fe^{2+/3+}$, which is sensitive to the amount of surface oxides (Figure 4C). This corresponds to an increase in the number of oxygen functional groups on the surface confirmed by the XPS results, as mentioned above. The value of ΔE_p for DA fell from 525 to 256 mV after UV/ozone treatment, as shown in Figure 4D. This is because the nanostructured carbon film surface has a relatively high surface area in comparison with the angstrom-level flat surface of the original nanocarbon film, since DA requires adsorption to the carbon surface to realize fast electron transfer.[34,35] These results indicate that the thornlike nanostructure itself has a high electron transfer rate for a redox species sensitive to the surface structure and/or chemistry.

DET-Type Bioelectrocatalysis for BOD and Cyt *c* on Thornlike Nanostructured Carbon Film. We used this thornlike nanostructured carbon film as an electrode for DET-type bioelectrocatalysis because a surface that is rough on the nano level could be advantageous in regard to bringing the enzyme redox center to the electrode surface and increasing the rate of electron transfer between the enzyme and the electrode. At the same time, it is well-known that the wettability of a carbon surface is crucial with respect to realizing DET between an enzyme and a carbon electrode.[2,18,36] Kano and co-workers[36] and Armstrong and co-workers[18] have studied the influence of the above properties on DET. Before enzyme modification, we prepared a hydrophilic flat nanocarbon film and a hydrophobic thornlike carbon film to evaluate the effects of both surface wettability and surface nanostructure on DET-type bioelectrocatalysis. The former was obtained using a 5 min UV/ozone treatment for nanocarbon. In contrast, the latter was obtained using short-time Ar milling

dx.doi.org/10.1021/ja108614d |J. Am. Chem. Soc. 2011, 133, 4840–4846

treatment of a hydrophilic thornlike carbon film. Table 1 summarizes the physical and electrochemical properties characterized by CV for various redox species (Figure 4 and Figure S5). As summarized in Table 1, these surface treatments were sufficient to change the surface status and enabled us to control the electron transfer of several redox species, especially $Fe^{2+/3+}$, which is very sensitive to the electrode surface status. With the four different surface conditions in Table 1, we can compare the efficiency of DET as influenced by the two major parameters of surface nanostructure and wettability.

Figure 5A outlines DET-type bioelectrocatalysis on the nanostructured carbon film with bilirubin oxidase (BOD), which has been investigated as a cathode for biofuel cells.[6,37] Figure 5B shows voltammograms of physically adsorbed BOD on the original and thornlike carbon films (the four kinds of carbon film electrodes listed in Table 1). The original nanocarbon exhibited a slight cathodic current of $-0.6\ \mu A\ cm^{-2}$ at 0.25 V, which we attribute to the DET-type bioelectrocatalysis current for BOD.[37] The cathodic current for the hydrophilic nanocarbon ($C^0 = 24.2\ \mu F\ cm^{-2}$) increased slightly to $-3.5\ \mu A\ cm^{-2}$. This is because a 5 min treatment changes the water droplet contact angle from 75 to 20° on the carbon surface while maintaining the original surface flatness. The above indicates that surface hydrophilicity improves the DET-type bioelectrocatalysis of BOD. It has been reported that sp^2 edge sites are essential for high DET efficiency of BOD.[18,38] On our nanocarbon films, the edge-site increase was observed through the higher electron transfer rates for $Fe(CN)_6^{3-/4-}$ and DA (which need edge sites for rapid electron transfer) relative to the original carbon surface. Therefore, both surface oxygen functional groups and sp^2 edge sites can increase the DET efficiency of BOD on carbon samples.

In contrast, the cathodic current on the thornlike carbon film was amplified greatly to $-102\ \mu A\ cm^{-2}$. This is comparable to the previously reported value,[37] indicating the very efficient electron transfer between our thornlike carbon film and BOD. Taking account of the hydrophilic surfaces of both carbon films with 5 min and 3 h UV/ozone treatments, we found that the nanostructured surface played a more important role than hydrophilicity in accelerating the DET between the type-1 site in BOD and the electrode. This is because the capacitance, which is correlated with hydrophilicity, increased only 1.4 times for our thornlike carbon film relative to the corresponding value for the hydrophilic carbon film in spite of a 30-fold increase in the catalytic current. In contrast, we obtained a cathodic current of $-1.3\ \mu A\ cm^{-2}$ for the hydrophobic thornlike carbon film, which is only slightly higher than that of the original hydrophobic flat film (Figure 5C). The value for our hydrophilic nanostructured carbon film was much higher than those of other carbon materials such as BDD and DLC, as shown in Figure 6.

In regard to the adsorption of BOD on the carbon surface, it has been reported that the adsorption of biomolecules on an sp^3-dominant carbon such as BDD is less than that on an sp^2-dominant carbon such as GC.[39] Therefore, it was possible that both the BOD adsorption and DET efficiency could have decreased on the thornlike nanocarbon because the sp^3 ratio increased from 0.4 to 0.6 after UV treatment. However, the DET efficiency of BOD actually increased on the thornlike nanocarbon surface. We also obtained the DET efficiency of BOD at BDD, which consists almost entirely of sp^3 carbon. The catalytic current of BOD-modified hydrophilic BDD at 0.25 V was $-7.4\ \mu A\ cm^{-2}$, which is ~7% of the DET current on the thornlike nanocarbon (Figure 6). This result also supports the idea that the sp^3 content is not the major factor governing the DET efficiency for BOD, and the nanostructure contributes greatly to the improvement in the DET efficiency in addition to the hydrophilic surface. Furthermore, the cathodic current of DET-type bioelectrocatalysis for BOD on our nanostructured film was 30 times greater than that on a hydrophilic flat surface despite a 1.5 times higher capacitance value. This indicates that the cathodic current increase is not solely due to the increase in adsorbed BOD. Since the cathodic wave is almost in a steady state, which indicates a diffusion-controlled reduction of O_2, a much larger current can be realized by constructing a gas diffusion electrode system.[40,41]

Table 1. Physical and Electrochemical Properties of the Original and Thornlike Nanostructured Carbon Electrodes with Different Surface Wettabilities

		Hydrophobic flat (Original)	Hydrophilic flat	Hydrophilic nano-structured	Hydrophobic nano-structured
Ra	Å	0.6	0.8	3.5	4.0
Contact angle	degree	75	20	6	52
O/C	—	0.04	0.08	0.13	0.06
C^0	$\mu F \cdot cm^{-2}$	12.3	24.2	34.1	18.7
$Ru(NH_3)_6^{2+/3+}$	ΔEp/mV	60	60	60	62
$Fe(CN)_6^{2-/3-}$		160	68	68	72
$Fe^{2+/3+}$		910	105	85	614
DA		525	357	256	223

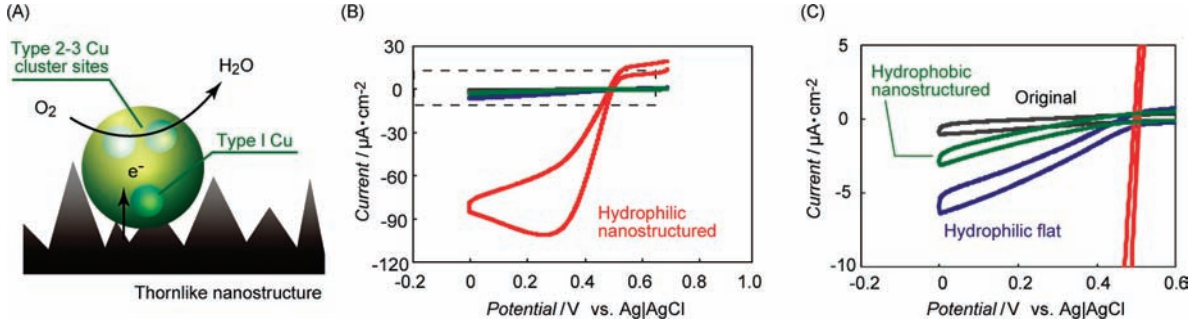

Figure 5. (A) Conceptual diagram of DET-type bioelectrocatalysis of BOD on the thornlike nanostructured carbon film. (B) Voltammograms of BOD physically adsorbed on original and nanostructured carbon films with different surface wettabilities [50 mM PB (pH 7.0), electrode area = 0.0314 cm^2, scan rate = 20 mV s^{-1}]. (C) Enlargement of the dotted square in (B).

dx.doi.org/10.1021/ja108614d | J. Am. Chem. Soc. 2011, 133, 4840–4846

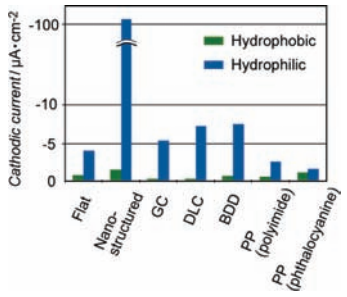

Figure 6. Cathodic current of DET-type bioelectrocatalysis for BOD with various carbon materials.

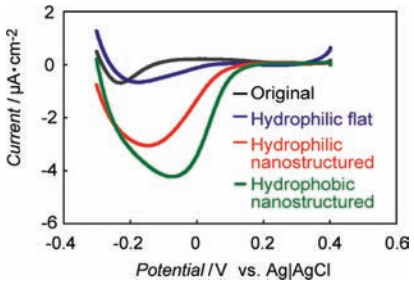

Figure 7. Background-subtracted voltammograms of 100 μM cyt *c* on original and nanostructured carbon films with different surface wettabilities [100 mM PB (pH 7.0), electrode area = 0.0314 cm^2, scan rate = 50 mV s^{-1}].

We also obtained voltammograms of DET-type bioelectrocatalysis for cyt *c* on the nanocarbon films, as shown in Figure 7. Cyt *c* is the best-studied enzyme in relation to DET[2,7,8,19] and is unlike BOD with respect to central metal, size, and isoelectric point. The voltammograms for the original nanocarbon film exhibited a slight cathodic current of -0.65 μA cm^{-2} at -0.22 V, which we attributed to the DET-type bioelectrocatalysis current for cyt *c*.[19,23] On the hydrophilic nanocarbon film, the cathodic peak potential shifted slightly from -0.22 to -0.17 V. However, the magnitude of the cathodic peak current changed very little in comparison with that of the original surface. Therefore, the surface hydrophilicity is a less important factor in terms of improving the DET-type bioelectrocatalysis with cyt *c*, which is unlike the case with BOD described above. In addition, the slight increase in the sp^3 ratio from 0.4 to 0.47 after 5 min of UV treatment did not affect the DET efficiency increase.

The cathodic peak current at -0.15 V for the hydrophilic thornlike nanostructured carbon film was amplified to -3.1 μA cm^{-2}, which is 4.8 times higher than that for hydrophilic flat carbon. For the hydrophobic thornlike nanostructure surface, the cathodic peak potential shifted to -0.06 V from -0.15 V and the peak current was amplified to -4.2 μA cm^{-2}, which is 1.4 times higher than that on the hydrophilic thornlike nanostructured surface. These results indicate that surface nanostructure and hydrophobicity are important for improving DET with cyt *c*. The results obtained with BOD and cyt *c* show that the surface nanostructure greatly improves both enzyme electrodes in spite of the enzyme dependency of surface wettability. Although a more detailed approach for improving DET with a surface nanostructure is still being studied, an increase in sp^2 edge sites would be one of the parameters because a nanostructured surface might have more sp^2 edge sites than the original hydrophobic surface, as suggested by the smaller ΔE_p for $Fe(CN)_6^{3-/4-}$ on the hydrophobic nanostructured film than on the original flat surface. Decreasing the average distance between the electrode surface and the central metal of the enzymes at the nanostructured surface also has good potential for improving the DET.

SUMMARY

We have described the fabrication of a thornlike surface structure on our nanocarbon film by employing UV/ozone treatment in ambient air without a plasma process or a mask. The obtained nanostructure was very efficient in greatly amplifying the DET-type electrocatalysis between the type-1 site in BOD and the electrode. In addition, we also observed the amplification of the DET-type bioelectrocatalysis for cyt *c* on our nanostructured carbon film. The size, height, and density of the thornlike structures could easily be tuned for a particular enzyme by changing the sputter deposition and UV/ozone treatment conditions to obtain a high electrocatalytic current.

ASSOCIATED CONTENT

Supporting Information. AFM images and XPS spectra of the nanostructured carbon film, AFM images of other carbon films before and after UV/ozone treatment, AFM images of the nanocarbon film treated by other techniques, and CV results for redox species on the nanocarbon film electrode. This material is available free of charge via the Internet at http://pubs.acs.org.

AUTHOR INFORMATION

Corresponding Author
niwa.o@aist.go.jp

ACKNOWLEDGMENT

This work was supported by Research Fellowships for Young Scientists from the Japan Society for the Promotion of Science and conducted at the AIST Nano-Processing Facility, supported by "Nanotechnology Network Japan" of the Ministry of Education, Culture, Sports, Science, and Technology (MEXT), Japan. This work was also supported in part by a Grant-in-Aid for Scientific Research (20245019) from MEXT, Japan.

REFERENCES

(1) McCreery, R. L. *Chem. Rev.* **2008**, *108*, 2646–2687.
(2) Katz, E.; Willner, I. *ChemPhysChem* **2004**, *5*, 1085–1104.
(3) Hartmann, M. *Chem. Mater.* **2005**, *17*, 4577–4593.
(4) Li, X.; Zhang, L.; Su, L.; Ohsaka, T.; Mao, L. *Fuel Cells* **2009**, *9*, 85–91.
(5) Tominaga, M.; Nomura, S.; Taniguchi, I. *Electrochem. Commun.* **2008**, *10*, 888–890.
(6) Willner, I.; Yan, Y. M.; Willner, B.; Tel-Vered, R. *Fuel Cells* **2009**, *9*, 7–24.
(7) Ivanov, I.; Vidaković-Koch, T.; Sundmacher, K. *Energies* **2010**, *3*, 803–846.
(8) Kim, J.; Jia, H.; Wang, P. *Biotechnol. Adv.* **2006**, *24*, 296–308.
(9) Masuda, H.; Watanabe, M.; Yasui, K.; Tryk, D.; Rao, T.; Fujishima, A. *Adv. Mater.* **2000**, *12*, 444–447.
(10) Yang, N.; Uetsuka, H.; Osawa, E.; Nebel, C. E. *Nano Lett.* **2008**, *8*, 3572–3576.
(11) Yang, N.; Uetsuka, H.; Osawa, E.; Nebel, C. E. *Angew. Chem., Int. Ed.* **2008**, *47*, 5183–5185.

(12) Strojek, J. W.; Granger, M. C.; Swain, G. M.; Dallas, T.; Holtz, M. W. *Anal. Chem.* **1996**, *68*, 2031–2037.
(13) Chiku, M.; Nakamura, J.; Fujishima, A.; Einaga, Y. *Anal. Chem.* **2008**, *80*, 5783–5787.
(14) Hirono, S.; Umemura, S.; Tomita, M.; Kaneko, R. *Appl. Phys. Lett.* **2002**, *80*, 425–427.
(15) Niwa, O.; Jia, J.; Sato, Y.; Kato, D.; Kurita, R.; Maruyama, K.; Suzuki, K.; Hirono, S. *J. Am. Chem. Soc.* **2006**, *128*, 7144–7145.
(16) Kato, D.; Sekioka, N.; Ueda, A.; Kurita, R.; Hirono, S.; Suzuki, K.; Niwa, O. *J. Am. Chem. Soc.* **2008**, *130*, 3716–3718.
(17) Mie, Y.; Suzuki, M.; Komatsu, Y. *J. Am. Chem. Soc.* **2009**, *131*, 6646–6647.
(18) Blanford, C. F.; Heath, R. S.; Armstrong, F. A. *Chem. Commun.* **2007**, 1710–1712.
(19) Haymond, S.; Babcock, G. T.; Swain, G. M. *J. Am. Chem. Soc.* **2002**, *124*, 10634–10635.
(20) Dronov, R.; Kurth, D.; Möhwald, H.; Scheller, F.; Lisdat, F. *Angew. Chem., Int. Ed.* **2008**, *47*, 3000–3003.
(21) Lisdat, F.; Dronov, R.; Möhwald, H.; Scheller, F.; Kurth, D. *Chem. Commun.* **2009**, 274–283.
(22) In *Three Bond Technical News*; Three Bond Co. Ltd.: Tokyo, 1987; Vol. 17, pp 1−10.
(23) Tominaga, M.; Hirata, N.; Taniguchi, I. *Electrochem. Commun.* **2005**, *7*, 1423–1428.
(24) Paik, N. *Surf. Coat. Technol.* **2005**, *200*, 2170–2174.
(25) Li, L.; Zhang, H.; Zhang, Y.; Chu, P.; Tian, X.; Xia, L.; Ma, X. *Mater. Sci. Eng., B* **2002**, *94*, 95–101.
(26) Bewilogua, K.; Wittorf, R.; Thomsen, H.; Weber, M. *Thin Solid Films* **2004**, *447−448*, 142–147.
(27) Park, C. K.; Chang, S. M.; Uhm, H. S.; Seo, S. H.; Park, J. S. *Thin Solid Films* **2002**, *420−421*, 235–240.
(28) Ferrari, A. C.; Robertson, J. *Phys. Rev. B* **2000**, *61*, 14095–14107.
(29) Ranganathan, S.; McCreery, R. L. *Anal. Chem.* **2001**, *73* 893–900.
(30) Banks, C. E.; Compton, R. G. *Analyst* **2006**, *131*, 15–21.
(31) Robinson, R. S.; Sternitzke, K.; McDermott, M. T.; McCreery, R. L. *J. Electrochem. Soc.* **1991**, *138*, 2412–2418.
(32) Martin, H. B.; Argoitia, A.; Angus, J. C.; Landau, U. *J. Electrochem. Soc.* **1999**, *146*, 2959–2964.
(33) Martin, H. B.; Argoitia, A.; Landau, U.; Anderson, A. B.; Angus, J. C. *J. Electrochem. Soc.* **1996**, *143*, L133–L136.
(34) DuVall, S. H.; McCreery, R. L. *J. Am. Chem. Soc.* **2000**, *122*, 6759–6764.
(35) Takmakov, P.; Zachek, M. K.; Keithley, R. B.; Walsh, P. L.; Donley, C.; McCarty, G. S.; Wightman, R. M. *Anal. Chem.* **2010**, *82*, 2020–2028.
(36) Kamitaka, Y.; Tsujimura, S.; Setoyama, N.; Kajino, T.; Kano, K. *Phys. Chem. Chem. Phys.* **2007**, *9*, 1793–1801.
(37) Tsujimura, S.; Kano, K.; Ikeda, T. *J. Electroanal. Chem.* **2005**, *576*, 113–120.
(38) Tsujimura, S.; Nakagawa, T.; Kano, K.; Ikeda, T. *Electrochemistry* **2004**, *72*, 437–439.
(39) Terashima, C.; Rao, T. N.; Sarada, B. V.; Tryk, D. A.; Fujishima, A. *Anal. Chem.* **2002**, *74*, 895–902.
(40) Kaisheva, A.; Iliev, I.; Kazareva, R.; Christov, S.; Wollenberger, U.; Scheller, F. *Sens. Actuators, B* **1996**, *33*, 39–43.
(41) Barton, S. C. *Electrochim. Acta* **2005**, *50*, 2145–2153.